INTERPRETATION OF RADIATION DATA FROM METEOROLOGICAL SATELLITES

W. NORDBERG

AUGUST 1968

GSFC — GODDARD SPACE FLIGHT CENTER
GREENBELT, MARYLAND

INTERPRETATION OF RADIATION DATA

FROM METEOROLOGICAL SATELLITES

W. Nordberg

August 1968

Lecture notes for WMO Regional Training Seminar on Interpretation of Meteorological Satellite Data.

GODDARD SPACE FLIGHT CENTER
Greenbelt, Maryland

INTERPRETATION OF RADIATION DATA

FROM METEOROLOGICAL SATELLITES

I. SENSING OF RADIATION

a. Physical Characteristics

Except for the tracking of balloons and the relaying of directly sensed measurements via satellite, observations of all physical properties of the lower atmosphere from orbit depend entirely on the sensing of electromagnetic radiation received from the earth's surface or from atmospheric constituents. Longwave radiation (infrared, millimeter and centimeter waves) is emitted into space by the earth and atmosphere, and its intensity is primarily a function of the temperatures of the emitting surfaces or gases but is also influenced by such factors as the morphology of a surface or the concentration and distribution of emitting gases along the optical path. Shortwave (near ultraviolet, visible and near infrared) solar radiation is scattered back into space by the earth and atmosphere; its intensity compared to the incident radiation, depends primarily on the nature and orientation of the scattering surfaces and, to some extent, on the size and concentration of the atmospheric scattering constituents. All measurements depend strongly on the geometry between the position of the satellite sensor, the area viewed on the earth, the local vertical, and, in the case of solar radiation, on the position of the sun.

The dependence of the radiation received by the satellite sensors on such atmospheric parameters as temperature, composition and particle size, and on the temperature and nature of the surfaces beneath the atmosphere is used to derive meteorologically significant information. Mathematical relations between these parameters and the sensed radiation are extremely complex, and cannot be stated explicitly for all cases. For example, the interpretation of conceivable satellite measurements of the intensity and polarization of solar radiation backscattered by the Earth depends not only on the nature of the reflecting surface, the size and distribution of particulate matter suspended in the atmosphere and the density of the atmosphere, but also on the assumptions of the laws for the various scattering process, e.g. Lambert's Law for backscattering from surfaces, Mie's Law for atmospheric particle scattering, Raleigh's Law for scattering by the molecular atmosphere, etc. In the case of infrared emission by a surface on Earth, the intensity I of the radiation measured by the satellite in a wavelength interval λ_1 to λ_2 is generally related to the temperature T and emissivity e of that surface by Planck's Law:

$$I \sim \int_{\lambda_1}^{\lambda_2} e(\lambda) \, B(\lambda, T) \, d\lambda \tag{1}$$

where λ is the wavelength of the measured radiation and $B(\lambda, T)$ is the Planck function. However, this radiation will be absorbed and reemitted by the atmosphere which depends on wavelength, temperature, pressure, atmospheric composition and a very precise knowledge of the absorption coefficients by the various gases. Many simplifying assumptions are necessary to describe these processes so that the meteorological parameters may be related to the radiation measurements. Cloud top and surface temperatures, estimates of the radiative balance at the top of the atmosphere, and broad averages of water vapor content in the upper troposphere, and of stratospheric temperature patterns were derived from radiation measurements by TIROS and early Nimbus satellites, using the best available models for infrared radiation transfer processes for water vapor, ozone, and carbon dioxyde and the assumption of blackbody emission by all surfaces, clouds and gases. (Allison and Warnecke 1966, Bandeen et al. 1965, Raschke and Bandeen 1967, and Kennedy and Nordberg, 1967).

Derivations of surface temperatures (cloud heights) were based on measurements of radiant emittance in spectral regions (4 and 11 microns) where the atmosphere is considered to be transparent ("windows"). Corrections for residual atmospheric absorption were shown to be small ($5°$-$10°C$ at 11 microns and $0°$-$2°C$ at 4 microns, Wark et al. 1962 and Kunde 1966) depending on the climatological assumptions made for carbondioxyde, water vapor, ozone and temperature distribution in the atmosphere. Similar assumptions were made when atmospheric temperature and water vapor were derived from radiation measurements centered on the absorption bands of CO_2 and H_2O at 15 and 6.3 microns respectively.

The determination of the balance between total emitted, telluric radiation and backscattered solar radiation, an important meteorological parameter, depends on the models used in extrapolating the satellite measurements of limited spectral range and response, and at selected angles of observation, to the entire range of the emission and solar spectrum and to the radiation flux in all directions. This method, which was applied to observations from TIROS and Nimbus in the 7-30 and 0.2-5 micron ranges, was successful only for emitted energy where models and assumptions developed by Wark et al. (1962) were used. Appropriate models for the angular and spectral dependence of reflected solar radiation are still lacking to derive a precise, absolute measure of the distribution of backscattered solar radiation from the satellite measurements.

More sophisticated analytical models are being developed to make more precise derivations of meteorological parameters not only of surface quantities such as temperatures or average atmospheric quantities, but also of the vertical distribution of atmospheric temperature, moisture, ozone, etc. To this end Dave and Mateer (1966) have developed a method to derive the amount and distribution of ozone in the stratosphere from measurements of solar ultraviolet radiation between 2500 and 3500Å backscattered to the satellite from the Earth's surface and atmosphere. This method will be explored on future Nimbus satellites. Considerable progress has been made (Wark and Fleming 1966) in expressing and solving relationships between the vertical distributions of temperature, water vapor, carbondioxyde and possibly ozone in the atmosphere and the emitted longwave radiation observable from satellites at very narrow spectral intervals (0.1 micron).

b. Sensors for "Mapping" of Radiation Patterns

Television cameras are ideal sensors to provide simple and instantaneous images of the intensity of reflected solar radiation which can be clearly related to cloud formations and terrain features. Because of the high intensity of visible sun light and because a large portion of that radiation is reflected by the Earth, high spatial resolutions can be achieved in this part of the spectrum. The resolution is given by the number of points in one individual picture frame and by the area to be covered by one frame. Present techniques permit each picture to be resolved into about 1000 by 1000 individual points. Used on a satellite such as Nimbus, covering most of the globe continuously during each day, this corresponds to a resolution of a fraction of a kilometer on the surface of the earth. Although imaging with television cameras provides excellent spatial resolution, it permits only poor relative intensity resolution (about ten "grey" levels) and practically no capability of absolute intensity measurements because of the great variability of sensitivity across the photosurface. Also, at this time, imaging with television cameras can be used only for visible solar radiation and is not suited for observations of emitted radiation which is necessary for nighttime mapping of cloud cover.

The same high spatial resolution, but much better photometric accuracy can be achieved with the use of scanning photometers (radiometers). Such photometers compose "images" by sequencially scanning their rather narrow field of view along a line on the surface of the Earth and by repeating each subsequent scan contiguous to the previous one. The "image" thus consists of a continuous strip, rather than of individual frames. Photometers always use scanning mirrors or similar rotating parts and are mechanically somewhat more complicated than television cameras. Visible radiation measurements showing cloud patterns from an altitude of over 36,000 km with a resolution of about 2-3 km (Fig. 1) were

obtained by Suomi (1967) with a scanning photometer on the ATS I satellite. Nighttime images of emitted infrared radiation at a wavelength of 4 microns were obtained with a "High Resolution Infrared Radiometer" (Foshee et al. 1965). The radiation maps displayed pictorially reveal the horizontal extent of clouds, contrasts between water and land and the temperatures of these surfaces. Earlier, on TIROS and again on Nimbus II, five channel scanning radiometers were flown to produce maps of the radiation field in the 11 micron atmospheric "window," the broad band ranges of total telluric emission (7-30 microns) and reflection (0.2-5 microns), the emission by water vapor at 6.3 microns, and the emission by carbon dioxide at 15 microns (Fig. 2, Nordberg et al. 1966). The choice of these intervals (channels) and their widths depend on the atmospheric parameter which is to be derived from the measurement and on the necessary sensitivity (signal to noise ratio) of the radiometer. On TIROS and Nimbus II the 11 micron window channels were about 5 microns and one micron wide, respectively. The water vapor and carbon dioxide channels were less than one micron wide. The fields of view of the five channel radiometers on TIROS and Nimbus corresponded to spatial resolutions of 65 km and 50 km respectively. Relatively high resolutions of intensity, about 100 levels or better (1-2°C) were typical for these radiometers. On Nimbus I the 4 micron radiometer had a spectral band width of about 0.8 microns and a field of view of about 0.5 degrees corresponding to a spatial resolution on the surface of the earth of about 10 km. Radiometers are now under development for day and nighttime operational mapping of radiation in the 11 micron window with much narrower fields of view. Spatial resolutions of about 5 km seem quite feasible within the next few years. Despite the very high relative intensity resolution the absolute accuracies of radiation measured by early TIROS radiometers over long periods of time (several months) were unsatisfactory because the calibration of the sensors did not remain stable for such long periods in space. Continuous inflight calibration, which was accomplished on Nimbus, is therefore very important.

At much longer wavelengths, in the microwave spectrum, scanning radiometers will produce images of emitted radiation from terrains, water surfaces and rain clouds. At wavelengths of greater than 1.6 cm radiation is received from depths a few centimeters below the surfaces and is not appreciably altered by the atmosphere or by non-precipitating clouds. Thus, the nature of land, ice and snow surfaces can be mapped more precisely and the presence of rain might be detected over relatively uniform ocean backgrounds. A radiometer operating at a wavelength of about 1.6 cm and providing a spatial resolution of about 50 km from a 1000 km orbit is now under construction. It is expected to be flown in the early 1970's (Thaddeus, 1966). Similar radiometers sensing radiation at wavelengths near 1.35 cm, where absorption and reemission by atmospheric water vapor occurs, may be developed to map patterns of atmospheric water vapor over oceans in the troposphere more reliably than can presently be achieved with infrared techniques.

c. Radiation Sensors for "Sounding" of the Atmosphere

Commensurate with the development of analytical methods to relate more rigorously the derived atmospheric parameters to the measured radiation quantities, instruments with higher spectral resolutions over a wide range of the solar and telluric spectrum are being developed. These spectrometers will provide intensity resolutions similar to previously flown radiometers but at much narrower spectral intervals. In the infrared, relative spectral resolutions ($\Delta\lambda$:λ) ranging from 1:100 to 1:500 will be achieved. This corresponds to a spectral width of 0.1 to 0.02 microns at a wavelength of 10 microns. In the near ultraviolet, absolute spectral resolutions of about 10Å are anticipated. Such spectral resolutions are required to infer, quantitatively; atmospheric water vapor, temperature and ozone. These instruments have not yet been flown on meteorological satellites, but their use is contemplated on future spacecraft. Their field of view will be fixed toward the satellite subpoint and will cover a continuous strip on the earth's surface, about 100-200 km wide, under the orbit of the spacecraft. Such coarse spatial resolution is dictated by the relatively long times (10-20 seconds) required to scan the desired spectral range. A variety of instrumental techniques will be used including conventional, fixed grating, multidetector spectrometers, Michelson interferometers, and spectrometers in which spectral separation is achieved by rotating wedges of continuous interference layers. (Hilleary et al. 1966, Hanel and Chaney 1966,[5] Hovis 1966). Improvements in spatial and spectral resolution by about one to two orders of magnitude can be expected when highly cooled infrared detectors (77°K) can be accommodated routinely on spacecraft. This will not be the case in the near future. Multi-channel instruments are also being considered in the microwave absorption band of molecular oxygen near 0.5 cm to measure atmospheric temperature distributions with sensitivities similar to presently developed infrared spectrometers. The major technological problem here is the high power consumption which is incompatible with present spacecraft technology. However, it seems promising that by the mid 1970's these power requirements can be satisfied.

Other, more exotic sensors have been proposed for the measurement of atmospheric density and wind. These include passive systems such as high precision star trackers (Fischbach 1965), or active systems such as doppler microwave receivers tuned to transmitters on "slave" satellites (Werbowetzki 1966) for measurements of atmospheric density profiles by the "occultation method," and radar techniques for possible wind observations over oceans (Pierson 1964). The density measurement methods are based on the fact that, when electromagnetic radiation passes through the atmosphere, its velocity of propagation is reduced due to the higher refractive index of the air, and its direction of propagation is bent, due to gradients of the refractive index across the ray path. The index of refraction μ is related to the atmospheric

5

density by $\mu = 1 + k\rho$, where ρ = density, k = constant for a given wavelength. Measuring the refraction of star light from a satellite during occulation by the Earth thus leads to a determination of the density profile of the atmosphere above the area where the ray is tangent to the surface of the earth. In the radio occultation method, a master satellite would continuously transmit to a small repeater satellite. The signal would be received and coherently retransmitted back to the master satellite where its frequency would be electronically compared with the transmitted frequency. The frequency difference relates to the change in the apparent ray path which deviates from the actual distance between the two satellites proportionally to the density of the atmosphere in the path. A precise measurement of the actual distance between a transmitter and receiver must be obtained from tracking the two satellites. For ray paths near the surface, the apparent path deviates from the actual path by about 1500 meters.

A method has been suggested by Pierson (1964) to infer surface wind fields over oceans by observing the heights of ocean waves. These can be mapped from a satellite by measuring the intensity distribution of radio signals transmitted by the satellite and backscattered by the ocean surface. For both the density and wind soundings, however, analytical models which realistically relate the radiation quantities to be measured to density and wind respectively are still lacking and more theoretical analyses, laboratory and field tests, and possibly exploratory spacecraft flights must be conducted before these measurements will yield useful observations of the atmosphere.

d. Radiation Sensing from Geosynchronous Orbit

Meteorological satellites orbiting at relatively low altitudes (1000 km) have one major disadvantage, even if they provide full global, and regular coverage such as the "sunsynchronous" TOS and Nimbus: The spacecraft will pass only once every 12 hours over the same region. This is the case especially at low latitudes. Such frequency of passes will generally suffice for large scale measurements of atmospheric parameters such as temperature, moisture, etc. However, observations of cloud patterns, which can be carried out so well with satellites, should ideally be made continuously, especially over areas where short lived mesoscale systems (tropical storms, tornados, thermally driven convective cells, etc.) dominate the weather. For that purpose the satellite should be in a "geosynchronous" orbit, i.e. the angular velocity of the spacecraft around the equator should be equal to that of the Earth around its axis; namely one revolution in 24 hours. Thus, relative to the earth's surface the spacecraft will remain stationary over whichever point along the equator it is inserted into that orbit. A geosynchronous orbit requires a distance of about 36,000 km from the Earth's surface. From that distance a major portion of the globe can be viewed continuously and permanently. Cloud observations from a geosynchronous

orbit were first carried out with the ATS-I satellite, launched in December 1966 over the Pacific Ocean at approximately 150°W. The view from ATS-I encompasses the entire Pacific Ocean and cloud systems with sufficient detail are resolved between the east coast of Asia and the west coasts of the Americas from the tropics to moderately high latitudes in both Hemispheres (Figure 1). The excessive distance from the Earth is also the major disadvantage of a geosynchronous orbit. The energy gathering power of the sensors must be enormous to resolve a small area element on the Earth's surface. Ironically the mesoscale systems whose observations require a geosynchronous orbit, because of their limited extent, also require very high spatial resolutions of the order of a few kilometers. By far the largest amount of energy for remote sensing is available in the visible part of the spectrum. Thus, at this time, only sensors operating in that part of the spectrum provide the spatial resolution necessary for the observation of mesoscale meteorological systems from geosynchronous orbits.

The ideal operational meteorological satellite system of the future should, therefore, consist of a set of spacecraft in two different orbits: a near earth, sunsynchronous orbit to provide regular quantitative observations of a variety of meteorological parameters every twelve hours with instruments of high spectral resolution; and a geosynchronous orbit to afford continuous high resolution imaging of weather patterns, especially of relatively short lived, mesoscale cloud formations, with broadband cameras or photometers in the visible or infrared.

II. ANALYSIS OF CLOUD PATTERNS OBSERVED IN INFRARED EMISSION

The intensities of emitted radiation measured in the infrared "windows" between 10 and 12 microns and at 4 microns provide an excellent means to derive the temperatures of surfaces "seen" by the satellite. Therefore, in the presence of clouds the emission to space occurs only from the top of the clouds where the temperatures are generally lower than at the surface. Consequently, the outgoing radiation is more intense over clear areas than over cloud tops from radiation measurements. The radiation intensity is a direct measure of the cloud surface (top), temperature. A unique relationship can be established between temperature and height either on the basis of climatologically assumed temperature profiles or from actual balloon sonde temperature measurements provided that it can be assumed that clouds do not penetrate above the temperature minimum at the tropopause. Pictorial displays of the radiometric temperature measurements in these windows have produced large scale "three dimensional" analyses of cloud heights. Cloud height differences of a few hundred meters can be detected and mapped by this method. Mapping of nighttime cloud patterns and

heights in the 4 micron window was especially successful with the NIMBUS satellites. The radiometer resolved about 100 steps of temperature (corresponding to shades of grey in the picture) from 200 to 310°K. Such synoptic presentations of cloud height, as well as cloud cover, give a still better insight into the dynamic of weather systems, especially their vertical extent, than can be obtained with cloud pictures alone. Simultaneous observation and mapping of cloud and weather systems in several spectral intervals on the same spatial scale though not at the maximum possible spatial resolution, further improves our ability to infer from the radiation patterns the location of air mass boundaries, the vertical extend, depth and stage of development of weather disturbances and, in some cases, even vertical motion and the course of the jet stream. The latter parameters are especially well observed if radiation patterns in the water vapor emission are included in the multispectral observations. The Nimbus Medium Resolution Infrared Radiometer (MRIR) observations consisted of 5 spectral bands; the visible (0.2-4.0 microns), total emitted infrared (5-30 microns), water vapor emission (6.4-6.9 microns), "window" emission (10-11 microns) and carbon di-oxide emission (14-16 microns). Examples of the measurements are shown in Figures 2 and 3. Figure 3 (top) shows a composite of the cloud picture observed by the window channel in the belt 30N-30S at local noon on 5 June 1966 except for the two passes near 140E and 170E which were obtained at local midnight. Although activity was relatively weak on this day the course of the Introtropical Convergence Zone can be followed around the entire globe. It generally follows the 10N parallel except over the Indian Ocean and Africa, where it dips down to the Equator. It is most intense over India and Indonesia and all but disappears over portions of the Pacific. Some lesser intensifications occur over Africa and South America. Over the Central Pacific, an interesting splitting into two narrow bands occurs.

The water vapor channel observations shown in the lower part of Figure 3 display dark regions on both sides of the cloud zone indicating strong subsidence. These wide, dry regions are indicative of the subtropical anticyclones. The warmest (driest) region observed in this channel is in the southern zone near 40W over eastern Brazil where very strong downward motion can be inferred. The narrow dark bands extending from east to west are generally associated with subsiding motion on the poleward side of the jet stream.

Figure 2 shows Hurricane Alma in two stages of its development observed by the MRIR in all five spectral bands. In the upper picture, the storm is fully developed and its shape is essentially the same in all five spectral bands. Comparison of the emitted and reflected radiation shows that the tail of the spiral consists mainly of high, but thin clouds while, lower, thick clouds are concentrated near the eye. In the water vapor channel note the sharp and long sector of dry air in the southwest section of the spiral. The cloud tops in the spiral are

generally very high, penetrating even into the carbon dioxide channel; digitally inferred temperatures are 223K and 232K in the water vapor and window channels, respectively. An entirely different picture prevails 4 days later (lower part of Fig. 2) when the storm is in its decaying stage. The brightest image occurs in reflected radiation with no noticeable spiral structure while in the window channel there is an indication of a wound up spiral but the clouds are relatively dark indicating low altitude. No trace of the storm can be seen in the CO_2 channel which maps the radiation from the upper troposphere. The storm has disappeared from the upper troposphere. Most noteworthy, however, the water vapor channel shows the most extensive and pronounced spiral with a dry band fully wound up several times within the storm, a typical sign of a mature or decaying circulation system.

Even if not complete in all aspects of meteorological analysis, such as air temperature and wind fields, this type of information obtained from cloud pictures provides an effective method of synoptic analysis and, at the very least, supplements analyses based on conventional observations.

The morphology of cloud patterns observed with television cameras and scanning infrared radiometers have provided the best source yet for inferring various aspects of the wind field, i.e., direction, speed and shear, from satellites. Also, studying the short term variation in the position of major cloud systems from synchronous altitudes (Figure 1) provides an excellent means to define the flow field associated with these cloud formations and to track the weather patterns which these clouds represent.

III. MEASUREMENTS OF THE EARTH-ATMOSPHERE
     RADIATIVE ENERGY BALANCE

The energy available for meteorological processes stems from global variations of heat stored in the atmosphere. The surplus or deficit in the amounts of radiative energy received from the sun and lost to outer space by the earth-atmosphere system plays an important role in the generation of these heat gradients. It is well known that the latitudinal variation of this net flux of radiation shows an excess of incoming solar radiation over outgoing radiation near the equator and a deficiency at the poles. Since the atmosphere exchanges heat, not only outward with space through radiation, but also as its lower boundary through conduction, friction, and through phase changes of water, it is impossible, at this time, to determine the entire energy budget of the atmosphere solely from satellite observations. Measurements of the net balance between incoming solar energy flux and outgoing longwave radiation at the top of the atmosphere, however, can be derived rather well from satellite observations. Some estimate of

the atmospheric energy distribution can be inferred on the basis of this radiative balance and with certain simplifying assumptions (Davis, 1964). The global distribution of the net radiation energy balance between the total absorbed solar radiation and the total emitted telluric radiation, its variation with latitude, longitude and time, may be derived from satellite measurements of portions of reflected solar and emitted long wave radiation at selected times of the day. Such measurements have been made with a number of satellites including Explorer VII launched in 1959 (Weinstein and Suomi 1961), TIROS IV, VII (Bandeen et al. 1965) and Cosmos 122 of the U.S.S.R.

The total amount of solar radiation absorbed by the earth-atmosphere is derived from satellite measurements of reflected radiation and from the assumption that one knows the total radiation received from the sun at the top of the atmosphere, and therefore, the quantity W which would be scattered back into space if the earth and atmosphere were a perfect, 100 percent efficient, isotropic reflector. Satellite radiometers are calibrated in terms of this quantity before flight. The backscattered energy at wavelengths between 0.2 and 4.0 microns from a given portion of the earth in a given direction is thus measured relative to W. Making the highly oversimplifying assumption that radiation is backscattered isotropically, one can derive the amount of radiation backscattered in all directions by this given area. This amount, expressed in percent of W, is referred to as the reflectance of the observed area. The absorbed energy can be calculated since that amount of the solar energy which is not scattered back into space must remain in the earth and atmosphere.

An example of the global variation of reflected solar radiation (albedo) of the earth and atmosphere, from which the absorbed radiation can be readily computed is shown in Figure 4, as observed by Nimbus II and averaged for the period 1 July - 15 July 1966. The latitudinal variation in the albedo given in Figure 4 as well as from other TIROS and Nimbus observations show relative maxima over the cloudy regions of the Intertropical Convergence Zone near the equator and over the clear but bright Sahara desert and minima over the clear oceanic areas in the subtropics. The albedo increases at high latitudes and is greatest over the cloud and ice covered polar regions. Absolute measurements of the total albedo of the earth derived so far from TIROS and Nimbus measurements leave much to be desired. In all cases the total amount of reflected radiation measured by the satellites was much too low (by about 40 percent) to balance the measured as well as the theoretically computed outgoing longwave radiation. Since such an inbalance cannot obviously exist on the long time scale observed by the satellites, it is suspected that the discrepancy stems from the models used in deriving the albedo, i.e. the total, omni-directional shortwave radiation flux, from the highly directional and partial satellite measurements.

Two relatively broad spectral intervals have been used on TIROS and Nimbus to derive the total emitted long wave radiation. One channel operated between 8 and 12 microns, the other between 7 and 30 microns. About 60 percent of the total emitted radiation is contained in the former channel, about 80 percent in the latter. Also, as in the case of solar radiation, a given spot of the earth is seen by the satellite only from one direction at a given time. Since, again, the emitted radiation varies in a complex manner with angle and with wavelength one must apply certain physical reasoning to extrapolate the total flux in all directions from the satellite measurements which were made in a limited portion of the spectrum and in one singular direction. These extrapolations are arrived at, in part, theoretically, in part, empirically. Results are shown in Figure 5 demonstrating the global distribution of total outgoing radiation derived from Nimbus II, averaged over the period 1 July to 15 July 1966. In general, these results confirm previous theoretical estimates of the global distribution of total emitted longwave radiation: A minimum of the outgoing radiation is found at the "meteorological" equator and maximum radiation is observed in the 20-30° latitude belts. The minimum is due to the extensive cloud cover associated with convective activity in the tropics which defines the meteorological equator, while the maxima in the two subtropical belts reflect the clear skies and warm temperatures associated with the extensive anticyclones in these regions. Beyond the subtropical belts, the total outgoing radiation decreases rapidly with latitude, especially toward the winter pole due to increasing cloudiness and decreasing surface temperatures. Further analyses of the distribution and variation of the emitted long wave radiation on smaller scales were performed by Jensen et al. (1966) on the basis of measurements from TIROS. These analyses demonstrated a likely correlation between fluctuations in the emitted radiation and disturbances in the tropospheric pressure and wind fields (Winston 1967).

IV. RADIATION OBSERVATIONS OF THE
    EARTH-ATMOSPHERE INTERFACE

The energy exchanges which take place at the lower boundary of the atmosphere have an equal bearing on the distribution of potential energy available to drive the atmospheric circulation as does the radiative net flux at the top of the atmosphere. Unfortunately, these exchanges which are not limited to radiative processes are not as accessible to direct and quantitative measurement as is the net flux of radiation of the upper boundary. Nevertheless, observation of patterns of blackbody radiances measured in the "window" portions of emitted longwave radiation can provide for the mapping of significant features, primarily temperature patterns, of the surfaces of land masses and oceans. Such mapping in the infrared windows resulted in precise measurements of ocean temperatures, the large scale observation of the distribution of ice and open

11

water around the polar regions, especially Antarctica, the identification of air masses in areas where advection of warm or cold air produced heating or cooling of the ground respectively, and the precise measurement of land surface temperatures from which qualitative inferences of the moisture content of the soil or the nature of its surface have been made (Nordberg 1965). Because of the strong interaction between the temperature of the ocean surface and the atmosphere, measurements of sea surface temperatures and mapping of ice-water boundaries are of particular meteorological interest. Future microwave measurements will undoubtedly make observations of ice, snow and water and of soil characteristics more versatile and useful as they will not be limited to cloud free areas.

Since the blackbody assumption for water surfaces is quite valid in both infrared windows the temperatures derived from radiation intensities relate directly to water surface temperatures. Therefore, in cloudless regions satellite borne radiometers can be used for global mapping of the surface temperatures of various bodies of water. The ability of the Nimbus II HRIR radiometer to map ocean temperature has been used on a large scale and the course of the Gulf Stream could be identified and plotted from satellite observations (Fig. 6, Allison et al 1967). Unfortunately, in many cases clouds obscure ocean areas of interest, so that global mapping of ocean surface temperatures in the infrared windows cannot be performed contiguously on a daily basis. Figure 7 is a radiation picture obtained by Nimbus I in the 4 micron infrared window of temperatures of ice and water surfaces in the Antarctic on 29 August 1965. The entire Atlantic sector of the continent is shown to be cloud-free, and the surface temperatures over the interior ice cap near the South Pole were determined numerically as 210° to 215°K. These extremely low temperatures were observed consistently during the lifetime of Nimbus I, from late August to late September. Near the edge of the continent surface temperatures increase markedly to about 240°K. The edge of the continent stands out sharply in the infrared picture because a band of apparently open water, in some parts about 100 kilometers wide, stretches along the coast of Queen Maud Land. Maximum temperatures of these areas are about 256°K. This indicates that the full instantaneous field of the radiometer was not viewing an entirely open area of water but that this band probably consists of broken-up ice. A wide shelf of floating ice stretches northward into the Weddell Sea and the Atlantic Ocean. The Weddell Sea ice can be easily distinguished from the inland ice because its surface temperature, 244°K is about 12° higher. Very narrow but distinct lines of warmer temperatures are found crisscrossing the shelf. These lines obviously are due to cracks in the ice, and in some cases they are over 200 kilometers long. The ice shelf extends to 57°S, where it is bounded by open water having temperatures of about 275°K.

The land surfaces are considerably more complex than sea or cloud surfaces. Therefore, under certain conditions, the temperatures derived from radiation

12

intensities measured over land surfaces depend not only on terrain heights, but also, to a large extent, on such parameters as heat capacity, conductivity, and moisture content. First, it must be determined whether the variations in radiation intensity are due to differences in actual ground temperatures or to variations in emissivity. In the radiation observations made in the infrared windows from Nimbus, most variations may be ascribed to differences in actual surface temperatures. No instances have been found in these observations where variations in surface emissivities could be clearly identified. Indeed, from experience with Nimbus one might conclude that effective detection of surface features by means of emissivity measurements from spacecraft will be possible only if the spatial and spectral resolutions of radiometric sensors are improved by several orders of magnitude over the capability of present instruments.

On the other hand, a number of topographic and geological features may be inferred from the measurements of thermal emission in the relatively broad spectral window bands. For example, the topography of the southwestern United States was repeatedly mapped by HRIR observations on Nimbus. Warm areas were identified as the low regions -- Death Valley and the Grand Canyon. Thus, observed temperature patterns corresponded to differences in terrain height. More quantitative interpretations of the temperatures over Death Valley revealed that the temperature difference of about 15°K measured by the satellite corresponded to an altitude difference of about 1800 meters between the valley floor and the surrounding highlands. The measured temperature decrease with altitude, about 8.3°K per kilometer, was in very good agreement with the expected temperature decrease in the free atmosphere (the atmospheric lapse rate).

A situation in which considerations other than topographic height changes are involved may be seen in Figure 8. The picture shows a very large portion of western South America as seen by the Nimbus I 4 micron radiometer on 14 September 1964, when much of the region was essentially free of clouds; exceptions were the Intertropical Convergence Zone north of 10°S, an extensive low altitude layer of stratus clouds along the entire west coast, a high-altitude cloud deck off southern Chile, and some smaller clouds along the eastern horizon. The broad, white (cold) band through the center of the picture corresponds to cold, high-altitude mountain ranges of the Andes. Average blackbody temperatures of 255°K are measured over the highest elevations, between 28° and 32°S. To the northeast there is a remarkably rapid transition from the cold highland, with average blackbody temperatures of 270°K, to the very warm Amazon Basin, with blackbody temperatures of 290°K. The warm waters of Lake Poopó (19°S) and Lake Titicaca (16°S) are clearly evident in the generally cold highlands. In the plateaus to the east of the mountains (30° to 35°S) and in northern Chile (24°S) remarkable fine structure in the temperature patterns may be observed. The crescent-shaped form near 23°S corresponds to the Salar de Atacama, a

13

salt flat in northern Chile. The discrete band of warm temperatures (273°K). surrounding the crescent stands out clearly, while the center is quite cold (263°K). The entire Salar has a fairly uniform altitude of about 2300 meters. Thus, on the basis of terrain height, there is no reason to assume the existence of a temperature difference between the center and the rim. Subsequent aircraft observations in this area showed a striking difference in the material on the top surface between the rim and the center of the Salar: the center consists of sintered salt while the edge is covered by vulcanic material which eroded from the surrounding high mountains. This material, which is much darker and coarser than the salt, is about 10 to 15°C warmer, because it absorbs more solar energy. Consequently, a sharp temperature gradient can be detected from the satellite.

A similar situation exists in near 32°S, 68°W, part of western Argentina as seen by the radiometer. Here, a nearly circular dark band about 5 kilometers wide and 40 to 50 kilometers in diameter indicates the existence of a high temperature zone. The cold temperatures (light spot) in the center of the band can be easily explained by topography. The center of the band corresponds to the Pie de Palo mountain range. The lowest temperature measured in the center of the band is 268°K and corresponds to the highest elevation, about 3000 meters, of the range. The temperature along the band is about 280°K—about 7° higher than the temperature of the surrounding desert. Since the band around the mountain is topographically no lower than the surrounding desert plateau, the explanation of the warmer temperatures must be found in the difference in heat storage between the desert sand and the rocks of the Pie de Palo mountains. A visual survey revealed that the contrast between the Precambrian rock formations of the Pie de Palo mountains and the Alluvial sand deposits of the surrounding desert is indeed very striking and occurs around the mountains approximately along the 1000 meter contour line. The dark band seen by the satellite approximately parallels this 1000-meter contour line. Furthermore, the temperature difference of 12°K between the warm band at 1000 meters and the cold top of the mountain, which rises abruptly to 3000 meters, yields an approximate lapse rate of 6°K per kilometer. This corresponds to the expected adiabatic lapse rate much more closely than the temperature difference of 6° between the desert plateau at about 800 meters and the mountain top does. That latter difference would yield a rather unrealistic lapse rate of 3°K per kilometer. Thus, the temperature of the desert at night is considerably lower than the air temperature because of the small heat capacity and low conductivity of the ground. This low soil temperature results in a temperature inversion in the air over the desert, while the solid rocks remain considerably warmer, resulting in the adiabatically decreasing temperature from the periphery to the center of the mountain.

V. ATMOSPHERIC TEMPERATURE AND MOISTURE

From measurements in certain, sufficiently narrow spectral intervals, one can infer either the temperature or the amount of constituents, such as water vapor or carbon dioxide, distributed with height in the atmosphere. The spectral region must be chosen such that the absorption coefficient k, which depends on pressure (p) temperature (T) and on the wavelength (λ) for a given constituent, is very large; e.g., near 6.3 microns for water, near 15 microns for CO_2.

The intensity of radiation, measured at the satellite, for an absorbing spectral interval $\Delta\lambda$ is:

$$I_{\Delta\lambda} = \int_{\Delta\lambda} \phi(\lambda) I_s \tau_s \, d\lambda + \int_{surface}^{top} \Psi(h) \, dh, \qquad (2)$$

where

$$\Psi(h) = \int_{\Delta\lambda} \phi(\lambda) B(\lambda, T) \, [\partial\tau(h,\lambda)/\partial/h] \, d\lambda$$

and

$$\tau(p, T, \rho, \lambda) = \exp\left[-\int_0^h k(p, T, \lambda)\rho \, dh \right]$$

is the transmission from the level h to the top of the atmosphere, ρ is the number density of the absorbing gas and the subscript s refers to the underlying radiating surface. Scattering has been neglected and it is also assumed that the satellite is viewing in the vertical. The quantity $\Psi(h)$ represents the contribution of different altitude levels to the measured outgoing radiation. Equation (2) shows that the total value of $I_{\Delta\lambda}$ consists of contributions of radiation emitted from the lower boundary (first term) and from a gas within the atmosphere above that boundary (second term). In spectral intervals of high absorptivity of that gas (in band centers or in line centers) only radiation emitted in the upper layers can penetrate the atmosphere to space, while in spectral intervals of less absorptivity radiation from lower layers can penetrate to space.

The second term in Equation (2) indicates that the radiation intensity in the interval $\Delta\lambda$ is given by the vertical distribution of the temperature and of the concentration of the absorbing gas in those layers. Kaplan (1959) proposed to determine the vertical temperature profile from simultaneous measurements in different spectral ranges of the 15 micron CO_2 band. In this case the concentration of the absorbing gas can be assumed as known because of the constant mixing ratio of carbon dioxide in the atmosphere. The term $\partial\tau/\partial h$ for the Ψ function in the second term of equation (2) then can be expressed as a function of height and wavelength only. The variation of this term with height (pressure) is shown for several wavelengths (wave numbers expressed in cm^{-1}) in Figure 9. The curves in Figure 9 show that the intensity of radiation transmitted to the satellite is distributed with height depending on the wavelength interval. Thus, if a number of radiance measurements can be made in narrow intervals over a spectral region ranging from the center to the wings of an absorption band, the radiation measured at each interval will be distributed according to the weighting functions of Figure 9 with maxima at different levels in the atmosphere. Such a set of measurements will contain information on the vertical temperature distribution. However, because of the large amount of overlapping in the weighting functions, the individual measurements in the set will be highly interdependent. For this reason solutions to the problem of obtaining temperature profiles from such a set of radiance measurements tend to be highly unstable, placing great demands on both the accuracy of the measurements and the mathematical techniques employed. Several methods have been developed for treating the problem including the linear approach by Wark and Fleming (1966) and a nonlinear method of King (1964). The latter method is highly objective, but is confined to a representation of the temperature profile consisting of a limited number of ramps. The method of Wark and Fleming is well suited for the incorporation of a maximum amount of a priori information; in its most sophisticated form, use is made of empirical orthogonal functions derived from existing measurements of atmospheric temperature.

Complete temperature profiles have not yet been measured from satellites, but plans for such measurements exist and encouraging results have been obtained from attempts at inverting radiometric data taken with balloon borne instruments (Hilleary et al, 1966).

If the temperature is known, then the vertical distribution of an absorbing gas e.g., water vapor can be obtained from a set of spectral measurements in one of its absorption bands. If measurements are made in the infrared the results will be disturbed by the presence of clouds, dust and haze layers because the transmission properties of ice crystals and water droplets in those layers will dominate the properties of the gases.

Meteorological Satellites (TIROS, Nimbus) to date have only performed measurements in one single and relatively wide spectral interval for each absorbing gas, carbon dioxyde and water vapor respectively. For example, for TIROS VII the single interval in which emission from CO_2 was measured ranged from 14.8 to 15.5 microns. The "weighting function" for this single channel was considerably wider (30 cm^{-1}) than those shown for narrow intervals (5 cm^{-1}) in Figure 9, and ranged from 10 km to 35 km with the maximum at 20 km. In this case the contributions to the radiation from an underlying radiating surface [first term in equation (2)] may be neglected if that surface lies at altitudes below about 10 km. Most radiative surfaces (cloud tops) can be assumed to be below about 10 km. Thus, the radiation measurements in the 15 micron channel may be interpreted as a measure of the average temperature of the atmosphere within that altitude interval which is "seen" by this channel where each atmospheric height level contributes to the average according to the weighting curve. Variations in the average temperatures in the lower stratosphere can be readily detected by the variations of the 15 micron radiation measurements. On a global scale, such patterns of stratospheric temperatures bear a strong relationship to stratospheric circulation (Fig. 10). In general, the temperatures derived from TIROS VII near the summer pole (65° latitude) were of the order of 240°K, decreasing towards the winter pole where the stratospheric temperatures were found to be about 200°K.

Analyses of the stratospheric temperatures on a regional scale have also shown several interesting features. An intense warm area over the North Pacific related to the well-known Aleutian anticyclone has been clearly identified and other features, such as sudden stratospheric warmings were observed (40°N, 60°E, Fig. 10). These stratospheric warmings have attracted considerable attention since they were first noticed over Berlin in 1950). Now, with the availability of continuous measurements of stratospheric temperatures over the whole globe by means of satellites, it will certainly resolve many questions regarding the extent and magnitude of their occurrences and their relation to the sudden changes in the stratospheric circulation. The satellite measurements are of particular interest since they enable the detailed study and comparison of these phenomena in both hemispheres.

Observed variations in the patterns of equivalent blackbody temperatures reflect very well the seasonal temperature cycle of the stratosphere in both Hemispheres and the fact that this cycle is exactly in phase with the variation of the declination of the sun. The stratospheric temperature fields, especially the variance of temperature along high latitude circles, are indicative of large scale horizontal eddies during winter in both Hemispheres (Kennedy and Nordberg 1967). The eddies, which are probably responsible for transporting heat and ozone to high latitudes, seem to develop in preferred locations around warm

air cells over the Aleutian Islands and over Australia in the respective Hemispheres. Wave number one dominates both of these eddies. The one in the Northern Hemisphere is considerably more intense and stationary than its Southern Hemisphere counterpart. In both Hemispheres eddy activity begins to increase at the atumnal equinox and intensifies about two months later, but in the Northern Hemisphere this activity ceases abruptly just before the vernal equinox while in the Southern Hemisphere it does not subside until about two months later. In both Hemispheres large scale eddy circulation is absent during the summer months. Because of the greater poleward heat transport during the winter by the horizontal eddies in the Northern Hemisphere than in the Southern Hemisphere, temperatures in the tropics follow an annual variation which is in phase with the Northern Hemisphere cycle. Tropical temperatures are appreciably higher during June than during December.

The single channel spectral interval in which emission from water vapor was observed with TIROS IV and Nimbus II extended from 5.8 to 6.9 microns and 6.4 to 6.9 microns respectively. The weighting function which gives Ψ in equation (2) as a function of height now depends on both the distribution of temperature and water vapor with height. A temperature profile is assumed on the basis of climatology or an independent measurement by balloons in the vicinity of the region observed by the satellite. In addition, in this spectral region, even for a very moist atmosphere, a considerable amount of radiation is observed from the underlying surface, cloud top or ground. Thus, the first term in equation (2) cannot be neglected, it must be determined from a simultaneous measurement in one of the window channels, usually at 10-11 microns. This always yields a temperature for the radiating surface at the bottom of the water vapor. Then, only a temperature gradient (lapse rate) must be assumed for the atmosphere above to give a complete temperature profile. However, the surface underlying the water vapor must be equally opaque to radiation in the window as well as the absorption channel. If this is not so, such as in the case of thin, high altitude cirrus clouds, serious errors may result in the water vapor measurements. Finally, since only one spectral interval is available in water vapor absorption, only the total amount of water vapor in the height interval where $\Psi > 0$ can be measured; the distribution function for the water vapor with height must be assumed or known independently. Usually, a "standard" water vapor distribution with height, such as constant relative humidity in the troposphere and a constant water vapor mixing ratio in the stratosphere, were assumed. This method was developed by Moller (1962). For most realistic distributions of water vapor $\Psi = 0$ at altitudes below 500 mb (6 km) and the weighting function has a maximum near 300 mb (9 km).

This method was applied to the observations from TIROS IV (Raschke and Bandeen 1967) which resulted in the determination of the average total amount

of water vapor above the 500 mb level over many areas of the globe (Fig. 11).
The measurement of water vapor amount, even only as an average quantity is
most important at these heights since conventional meteorological radiosondes
become generally quite unreliable for water vapor measurements in the upper
troposphere.

The horizontal distributions of the water vapor mass in Figure 11 show a
pattern which is similar to that of the temperature. Both quantities decrease
from the meteorological equator in poleward direction. Highest amounts of
water vapor of more than 0.3 g cm^{-3} have been found over regions known to
have large amounts of precipitation. Those are South-East Asia (varying with
Monsoon-period), South America and Central Africa.

VI. OUTLOOK

Meteorological satellites so far have carried single and multi-channel
radiometric sensors and television cameras and have provided highly useful
meteorological information by:

1. Mapping the large scale distribution of cloud patterns, both in day and
   night, and determining the overall cloud top heights.

2. Determining the global distribution of energy sources and sinks in the
   earth-atmosphere system, namely the difference between the solar
   energy absorbed and the infrared energy emitted by the earth and the
   atmosphere.

3. Determining the global distribution of mean temperatures in the strato-
   sphere during a full seasonal cycle, and the distribution of water vapor
   in the upper troposphere.

The meteorological experiments carried out by satellites have so far been
limited to broad band radiometry, providing information only on cloud cover,
upper troposphere moisture fields, and on selected features of the circulation
inferred from the cloud, moisture and temperature patterns.

The next step in this field is to increase the spectral resolution of the
sensors, i.e., to make spectrometric measurements of temperature and moisture
distribution with height. Over oceans, atmospheric water vapor concentrations,
could be measured by microwave radiometers at wavelengths near 1.35 cm.
This wavelength range would be free of the interference encountered by thin
cirrus clouds in the infrared.

Another atmospheric parameter which can be usefully observed from the satellite is the distribution of ozone in the stratosphere. Because ozone is a strong absorber of the ultraviolet radiation, the measurements by a satellite of either direct or backscattered sunlight after its passage through the atmospheric ozone can be used for the deduction of the ozone distribution in the atmosphere.

The measurement of "sferics," the radio frequency emissions by electrical discharges from clouds, is still another domain in which satellite observations could contribute significantly. The detection and mapping of sferics may indicate areas of strong vertical motion related to tropical storm development and such phenomena as strong winds, heavy rainfall and turbulence.

It must be mentioned that the most important meteorological parameters, namely the surface pressure and the direction and velocity of the wind near the ground, cannot be accurately measured by instruments on-board a satellite at this time. The way in which the satellite can provide this information is by acting as a data collector and relay. Pressure and wind of the lower troposphere would be measured by a series of strategically placed sensors on the ground and in balloons, and the information from these detectors would be transmitted to the over-passing satellite which could locate and track the balloons and relay the sensor data to the analyst at a central weather station.

All these considerations will be part of future meteorological satellite programs, but their implementation is certainly a matter of formidable technological effort and will take at least the remainder of this decade to be completed.

REFERENCES

Allison, L., and G. Warnecke, (1966): The Synoptic Interpretations of TIROS III Radiation Data Recorded on 16 July 1961. Bull. Amer. Meteor. Soc., 47, 374-383.

Allison, L., G. Warnecke, L. Foshee and J. Wilkerson (1967): An Analysis of the North Wall of the Gulf Stream Utilizing Nimbus II HRIR Measurements, presented at the 48th Annual American Geophysical Union Meeting in Washington, D. C., April 1967.

Bandeen, W. R., M. Halev and I. Strange, (1965): A Radiation Climatology in the Visible and Infrared from the TIROS Meteorological Satellites. NASA TND-2534, 1-30.

Dave, J. V. and C. L. Mateer, "The Determination of Ozone Parameters from Measurements of the Radiation Backscattered by the Earth's Atmosphere," Jour. of Atmosph. Sci. to be published July 1967.

Davis, P. A., (1964): Satellite Radiation Measurements and the Atmospheric Heat Balance, Stanford Research Institute, Final Report Contract NAS-5-2919, July 1964.

Fischbach, F. F., A Satellite Method for Pressure and Temperature Below 24 km, Bull. Amer. Meteor. Soc., 46, No. 9, 1965, pp. 528-32.

Foshee, L. L., I. L. Goldberg and C. E. Catoe, (1965): The High Resolution Infrared Radiometer (HRIR) Experiment: Observations from the Nimbus I Meteorological Satellite, NASA SP-89, pp. 13-22.

Hanel, R. and L. Chaney (1965): The Infrared Interferometer Spectrometer Experiment. NASA Goddard Space Flight Center Document X-650-65-75.

Hilleary, D. T., E. L. Heacock, W. A. Morgan, R. H. Moore, E. C. Mangold, and S. D. Soules (1966): Indirect Measurements of Atmospheric Temperature Profiles from Satellites; III The Spectrometers and Experiments, Monthly Weather Review, 94, 367-377.

Hovis, W., (1966): A Proposal for Water Vapor Determination from NIMBUS D, NASA Goddard Space Flight Center, Greenbelt, Maryland, April 1966.

Jensen, C. E., J. S. Winston, and V. R. Taylor, 1966: 500-mb Heights as a Linear Function of Satellite Infrared Radiation Data, Monthly Weather Review, 94, 641-649.

Kaplan, L. D. (1959): Interference of Atmospheric Structure from Remote Radiation Measurements, J.O.S.A., 49, 1004-1007 (1959).

Kennedy, J. S., W. Nordberg (1967): Circulation Features of the Stratosphere Derived from Radiometric Temperature Measurements with TIROS VII Satellite, submitted to the Journal of Atmosph. Sciences.

King, J. I. F. (1964): Inversion by Slabs of Varying Thickness, J. of Atmos. Sci. 21, 324-326.

Kunde, V. G. (1965): Theoretical Relationship Between Equivalent Blackbody Temperatures and Surface Temperatures Measured by the Nimbus High Resolution Infrared Radiometer: Observations from the Nimbus I Meteorological Satellite, NASA SP-89, pp. 23-37.

Möller, F. (1962): Einige vorläufige Auswertungen der Strahlungsmessungen von TIROS II. Arch. Meteor. Geophys. Biokl., Series B, 12, 78-93.

Nordberg, W. (1965): Geophysical Observations from Nimbus I. Science, 150, No. 3693, 559-572.

Pierson, W. J., "Power Spectrums for Fully Developed Wind Seas," J. Geographical Res., Vol. 69, No. 24, pp. 5181-5203, 1964.

Raschke, E and W. R. Bandeen (1967): A Quasi-Global Analysis of Tropospheric Water Vapor Content from TIROS IV Radiation Data, to be published in the Jour. Applied Meteorology, Vol. 6, June 1967.

Suomi, V. E. (1967): For a description of cloud photographs from the ATS satellite refer to: [Robert H. McQuain: ATS-I Camera Experiment Successful, Bull. of the American Meteorological Society, Vol. 48, No. 2, February 1967, pp. 74-79.]

Thaddeus, P. (1966): A Microwave Radiometer for the Nimbus D Meteorological Satellite. Proposal NASA Goddard Space Flight Center, GISS, 2 August 1966.

Wark, D. Q., G. Yamamoto and J. H. Lienesch (1962): Methods of Estimating Infrared Flux and Surface Temperature from Meteorological Satellites. J. Atm. Sci., 19, 369-384.

Wark, D. Q. and H. E. Fleming (1966): Indirect Measurements of Atmospheric Temperature Profiles from Satellites: 1. Introduction, Monthly Weather Review, 94, 351-362.

Weinstein, M., and V. E. Suomi (1961): Analysis of Satellite Infrared Radiation Measurements on a Synoptic Scale. Monthly Weather Rev., Vol. 89, No. 11, Nov. 1961.

Werbowetzki, A., Refraction Data with Multiple Satellites, Bull. Am. Met. Soc., Vol. 1, 47, p. 199, 1966.

Winston, J. S., Planetary Scale Characteristics of Monthly Mean Long-Wave Radiation and Albedo and Some Year to Year Variations. Monthly Weather Review Vol. 95, No. 5, May 1967, pp. 235-256.
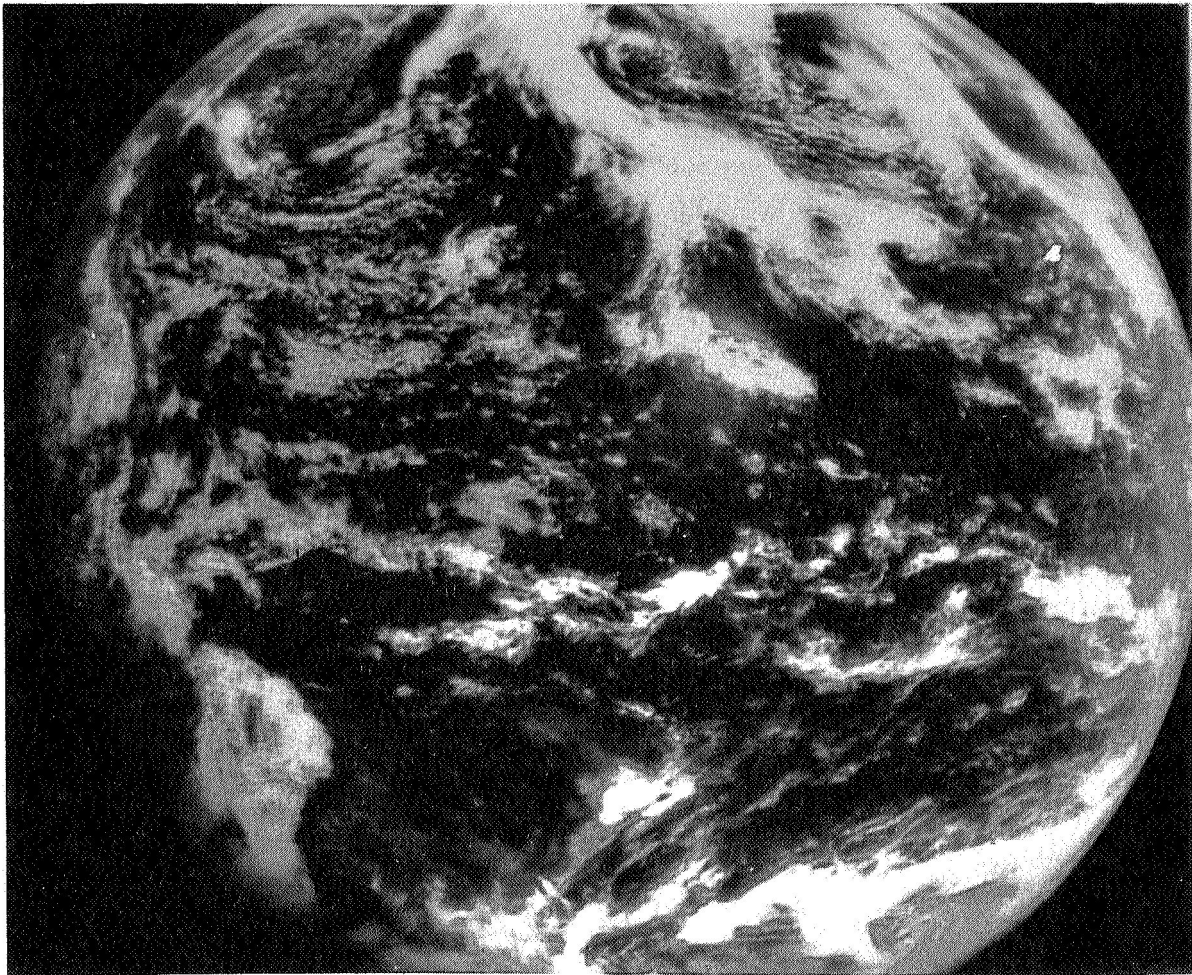
Figure 1—Cloud cover observed by a scanning photometer aboard ATS-I satellite over the Pacific Ocean on 11 Dec. 1966. The view extends from about 60°N to 60°S (top to bottom) and from the South China Sea (left) to the Atlantic Ocean (right). Cloud formations associated with major storms can be seen over eastern North America, the North Pacific Ocean, and the South Pacific Ocean. The peninsula of Southern California and the Southwestern United States and Mexico can be recognized in the cloud free area indicating high atmospheric pressure. Smaller scale cloud formations in the tropics are indicative of dynamic processes in these regions especially when their short term variation is analyzed.
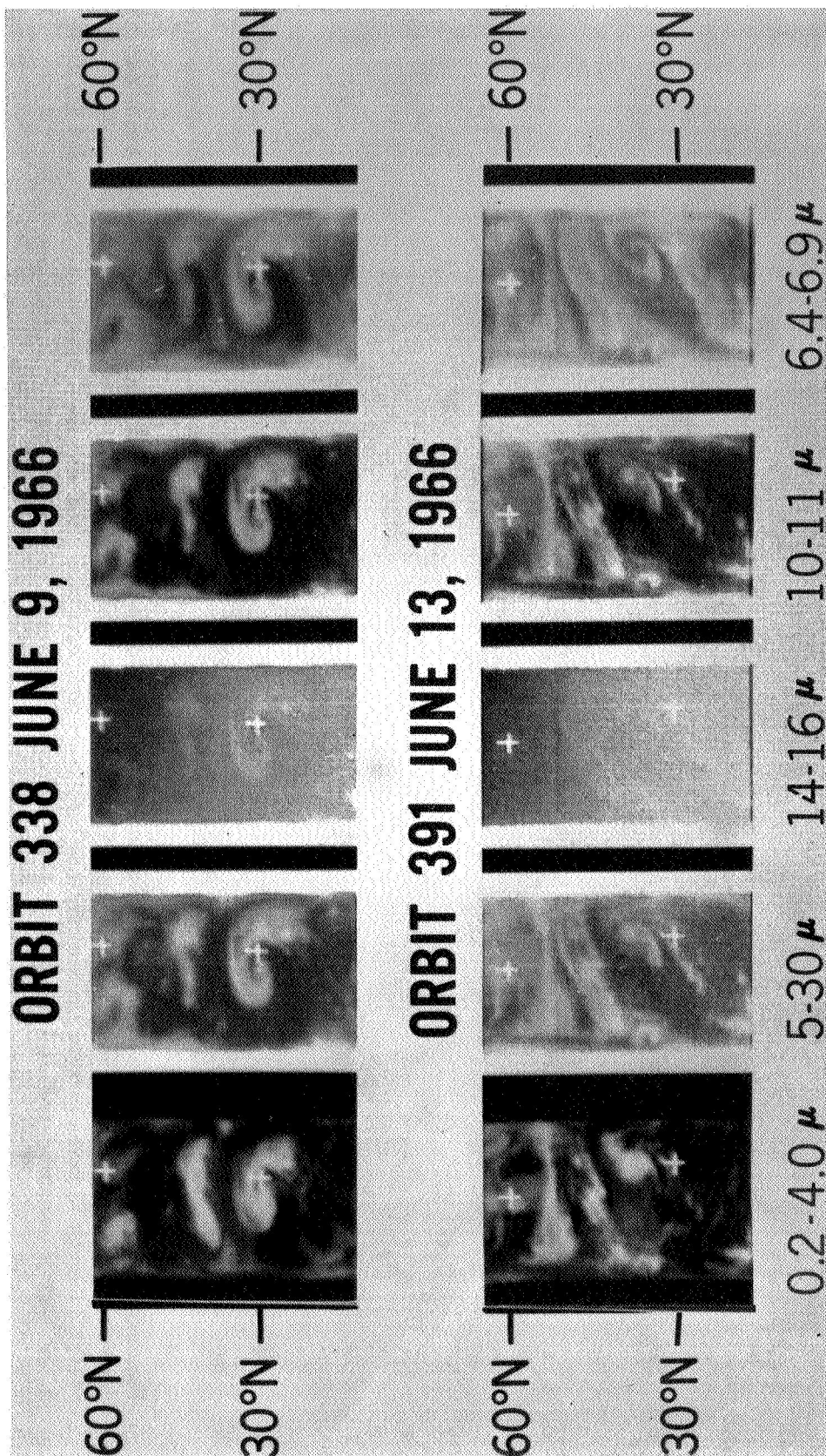
Figure 2—Observations of hurricane Alma in each of the five spectral regions during local noon on 9 June (upper picture) and local noon on 13 June (lower picture). In the upper picture the storm was located near 30°N, 80°W. In the lower picture it was located near 40°N and 70°W.
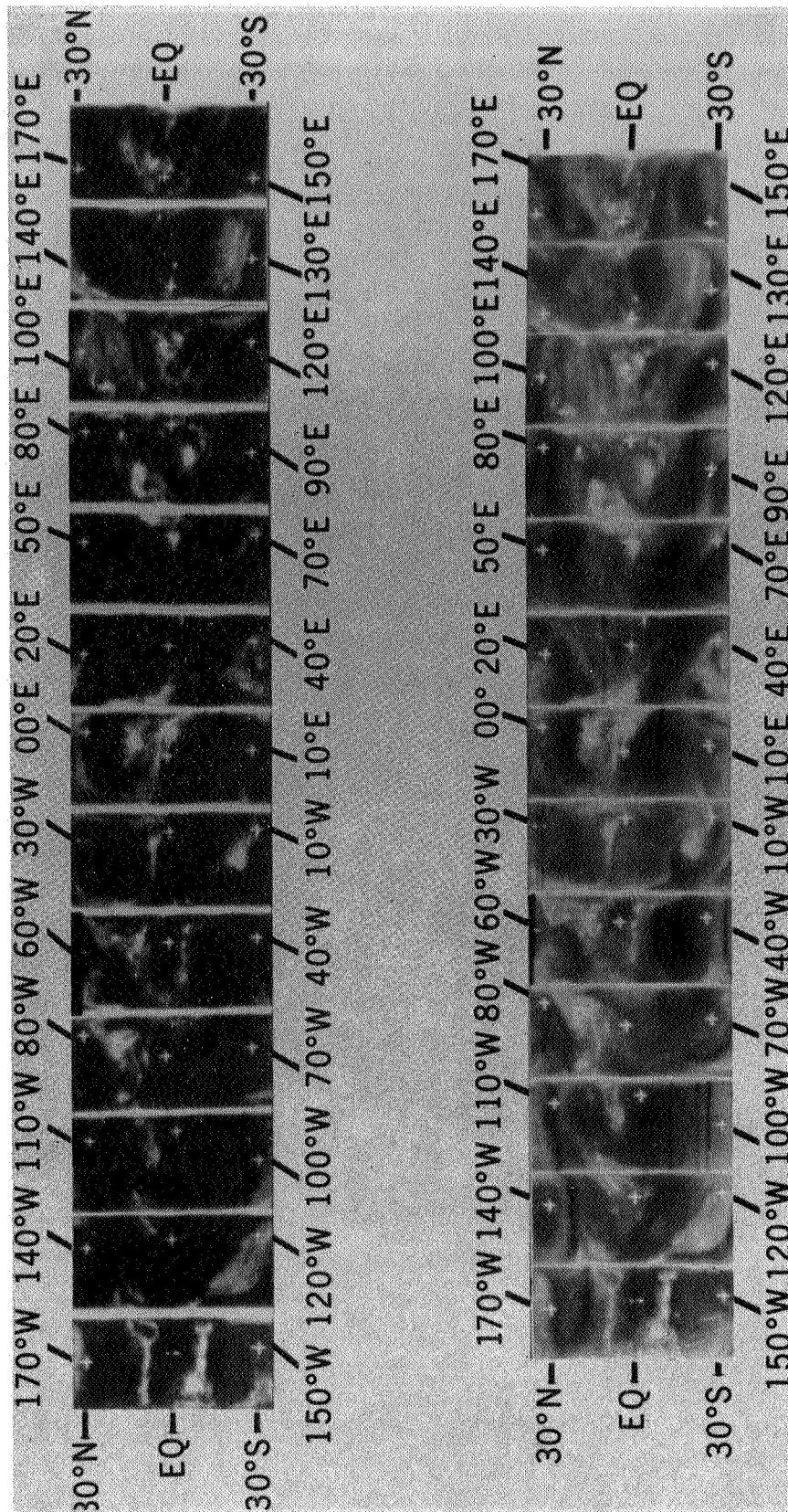
Figure 3—Cloud formations around the globe between 30°N and 30°S observed in the MRIR window channel (upper band) and in the water vapor channel (lower band) of Nimbus II. Each band is composed of thirteen orbital passes. Reading from right to left, passes 3 through 13 were observed sequentially near local noon on 5 June 1966. Because daytime data over longitudes E 130° to E 170° were not acquired, passes 1 and 2 shown at the right were observed 12 hours later near local midnight.
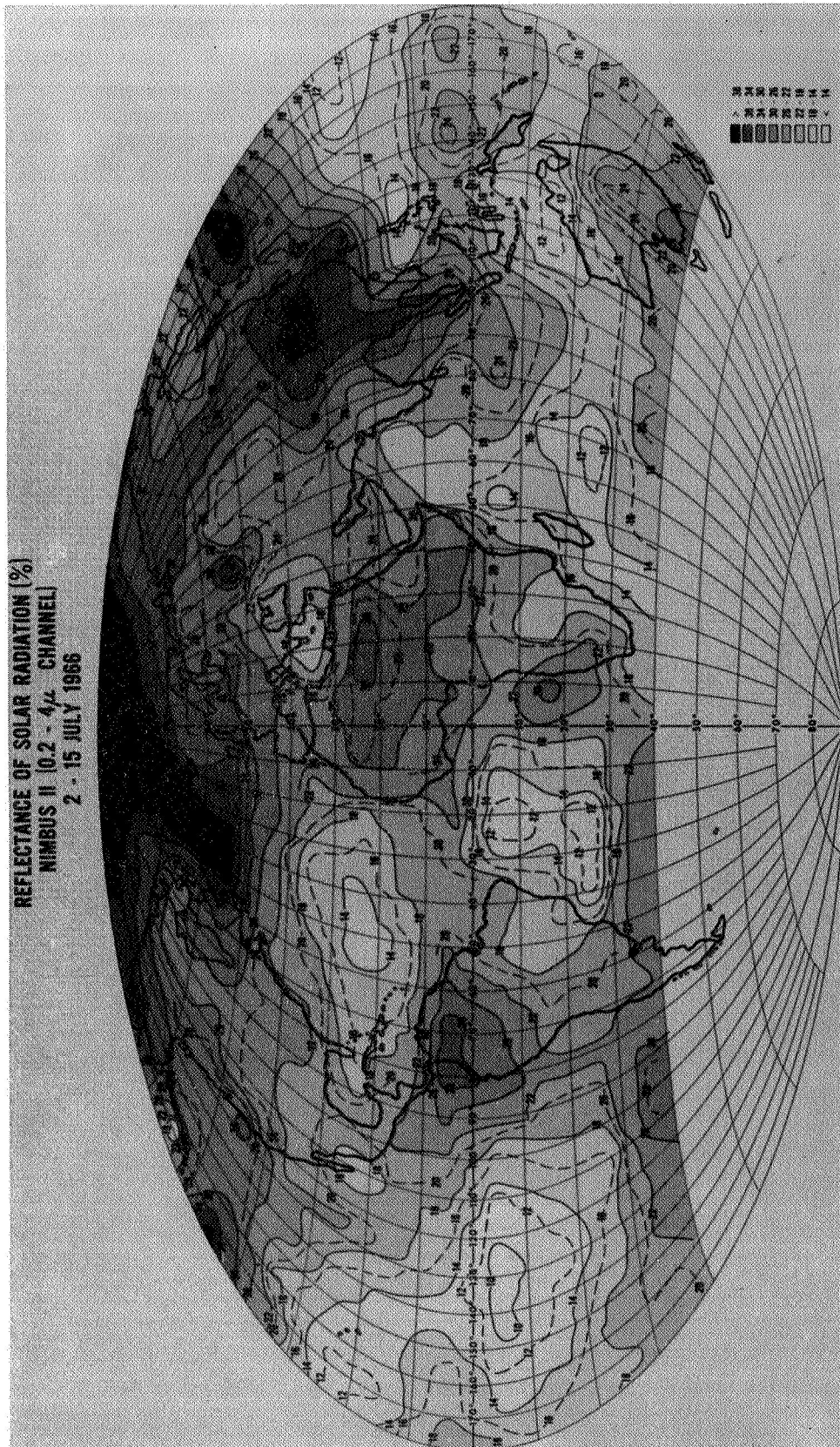
Figure 4–Reflectance of Solar Radiation (percent) from Nimbus II MRIR 0.2-4 micron Channel 2-15 July 1966.
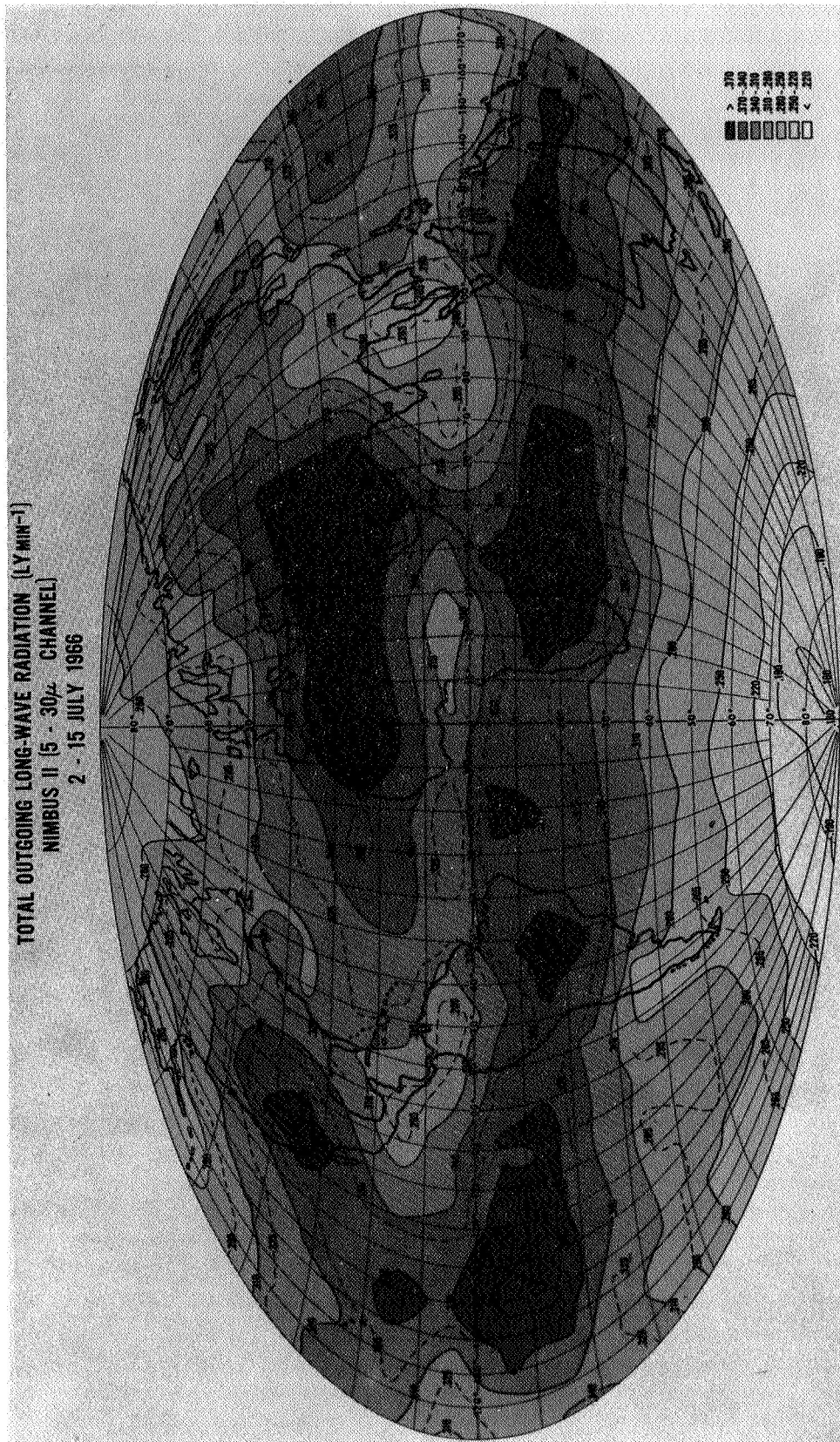
Figure 5—Total Outgoing Longwave Radiation ($LY min^{-1}$) from Nimbus II MRIR 5-30 micron Channel 2-15 July 1966.

28
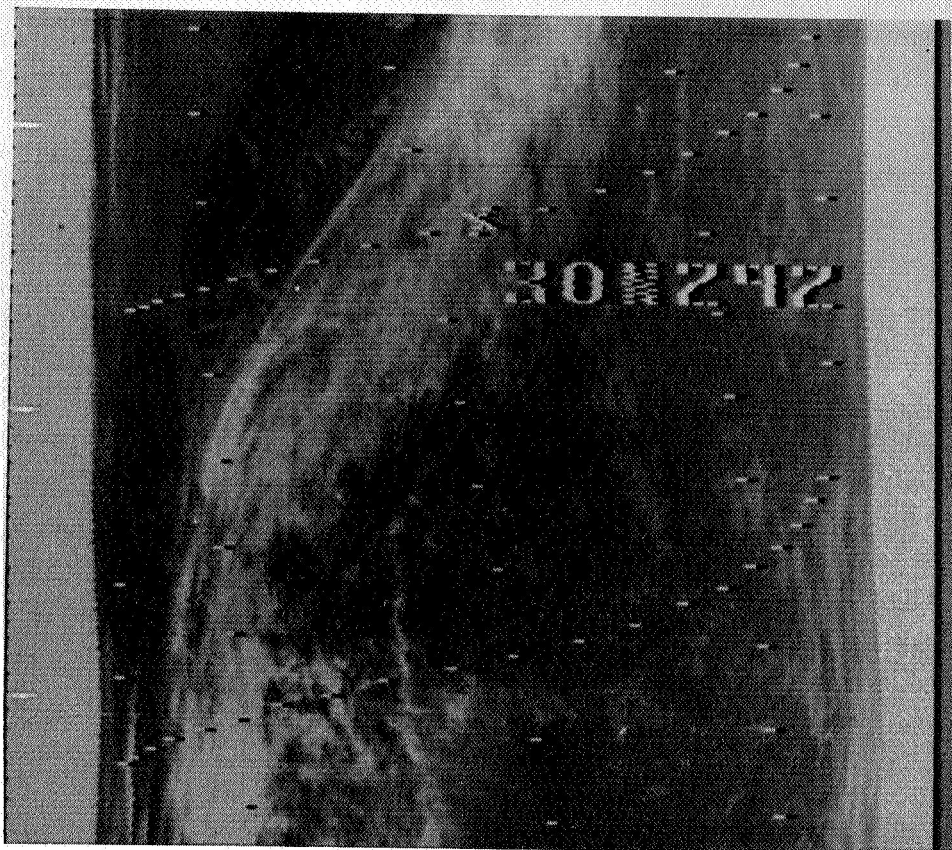
Figure 6—Nimbus II HRIR observation of the Gulf Stream near local midnight on 2 June 1966. The Gulf Stream is represented by the dark streak of warm water (298°K) in the upper left stretching from southwest to northeast. The streak is bounded sharply by colder water on the left. On the right the boundary toward the colder water is more gradual. The number in the center refers to 30°N, 292°E. The sharp temperature difference on the left amounts to about 5°C. A large cloud band is located to the east through the center of the picture. The land mass of the Eastern Seaboard of the United States is differentiated from the water by still colder temperatures (very light shades) along the left edge of the picture. At midnight the land mass is much colder than the water.
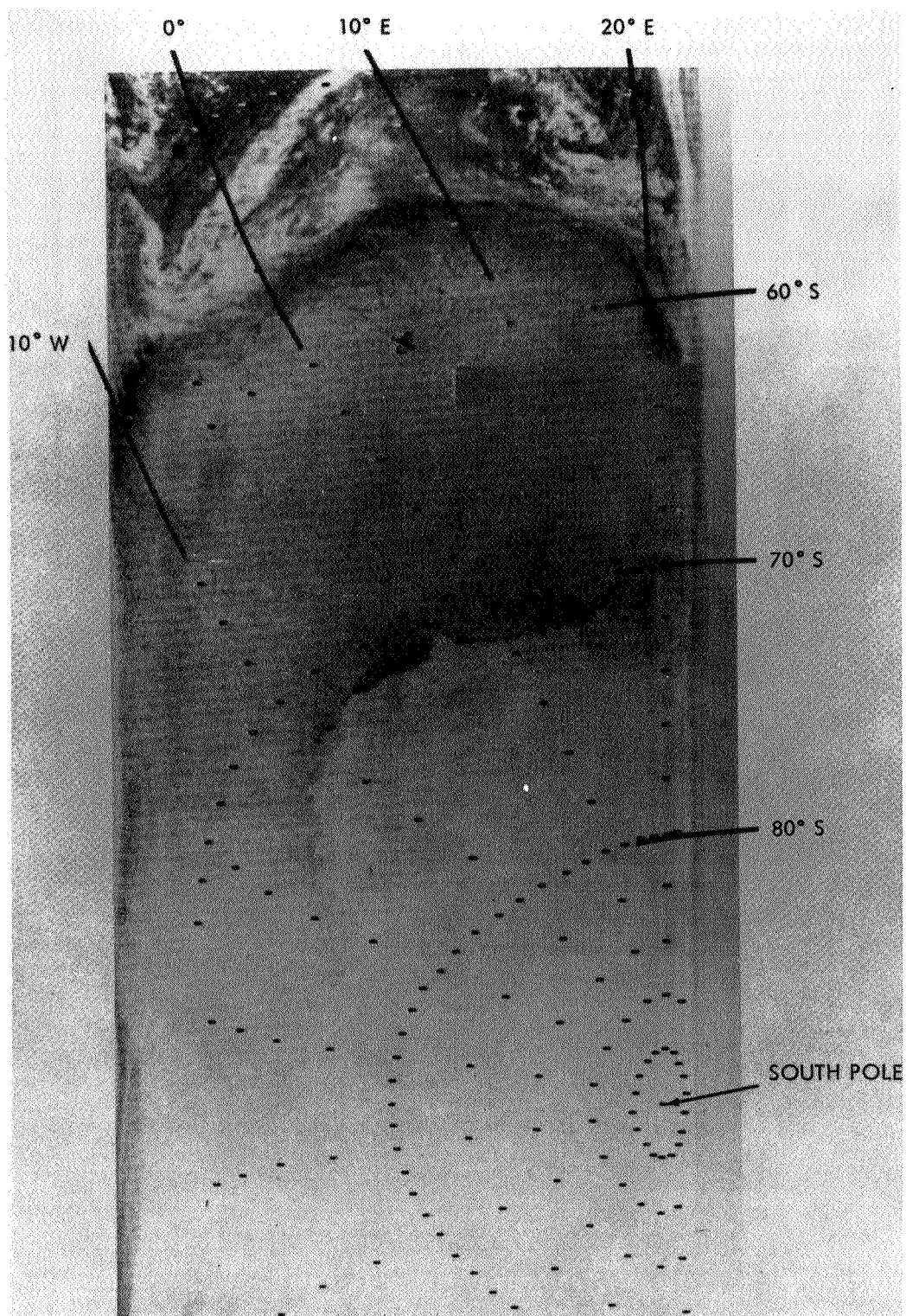
Figure 7—Nimbus I HRIR radiation picture made from above Antarctica at about midnight on 29 August 1964.
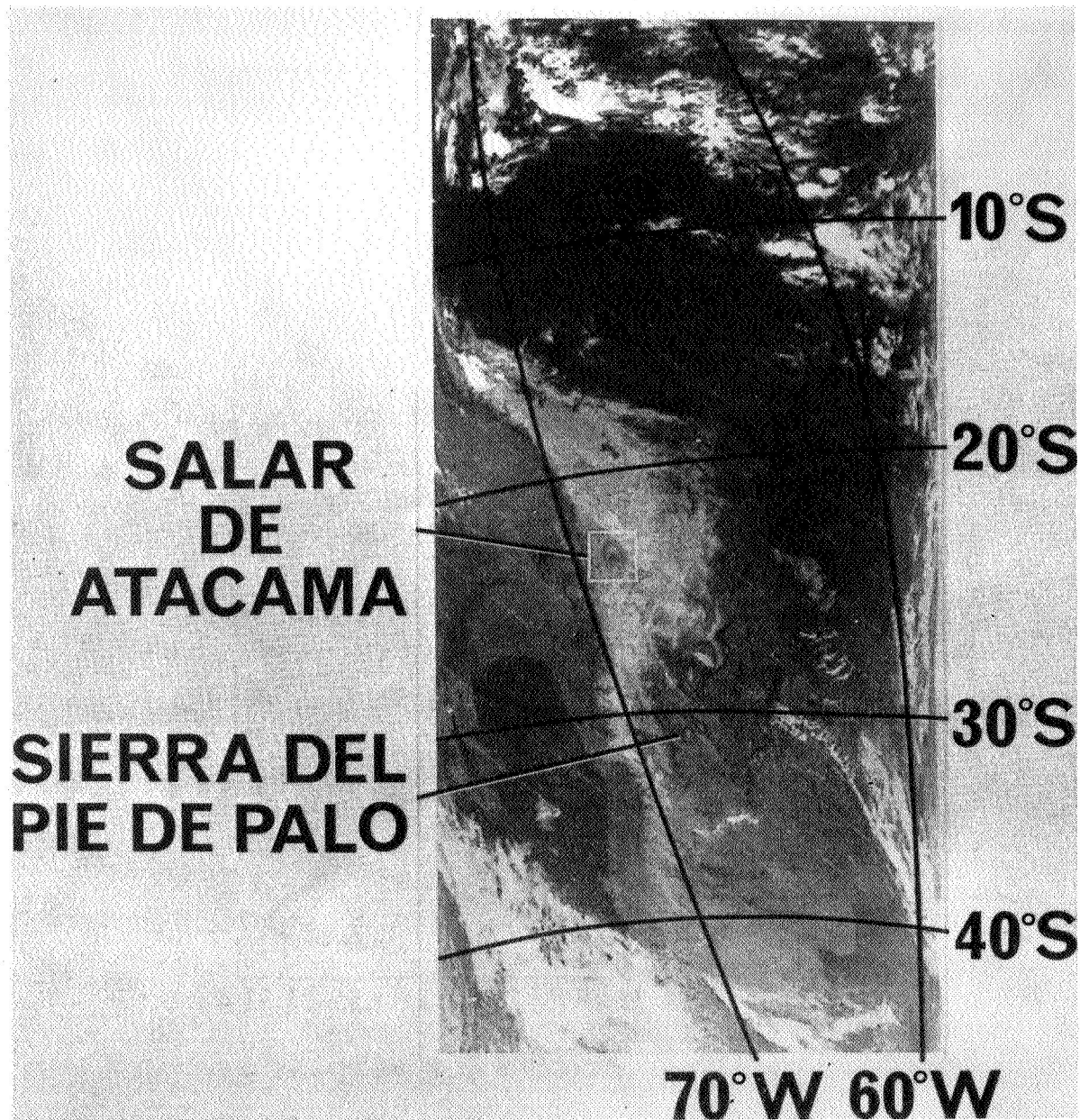
Figure 8—Nimbus I HRIR radiation picture made from above South America at about midnight on 13 September 1964.
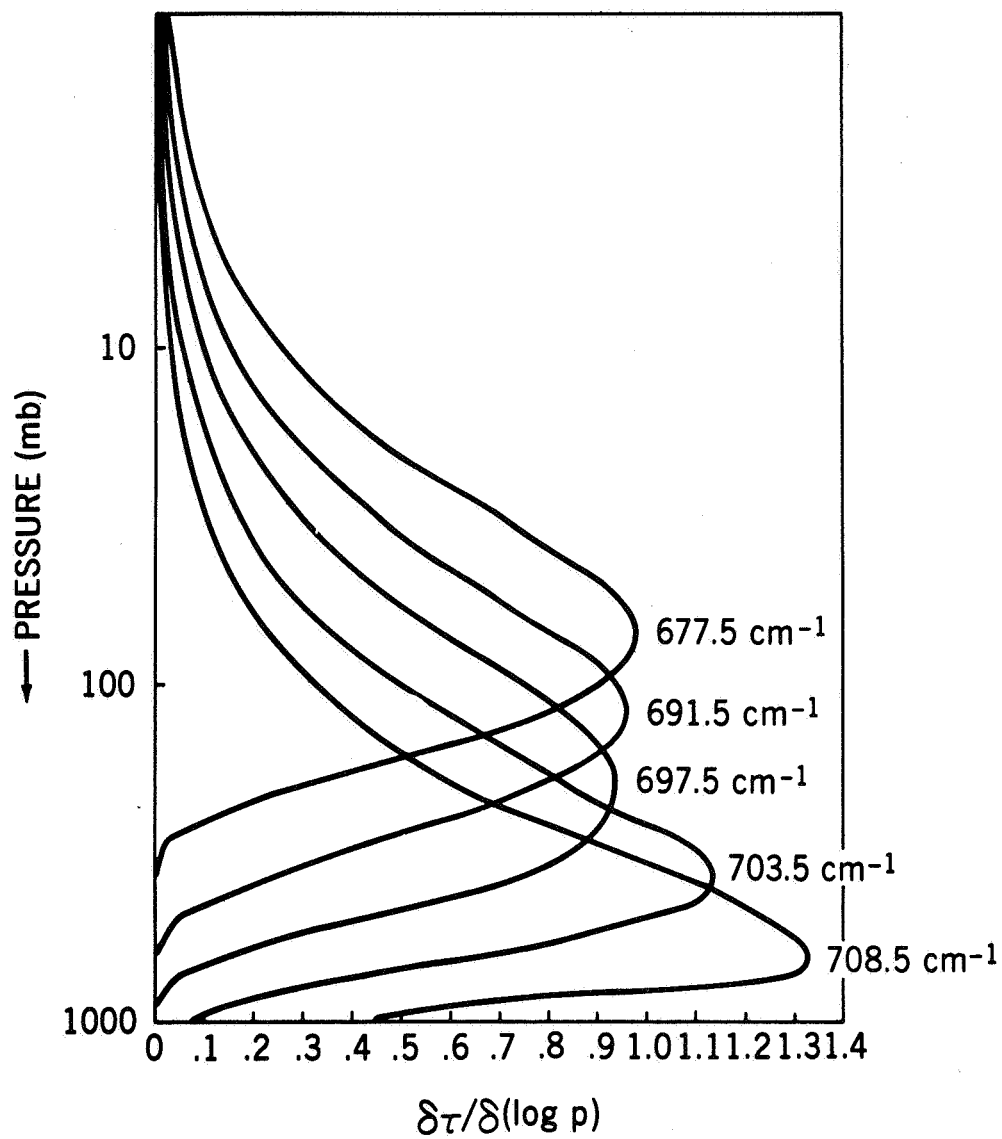
31

Figure 9—Fifteen micron carbon dioxide absorption band weighting functions. The 5 cm^{-1} wide spectral intervals were chosen with mid-points at the indicated wavenumbers.
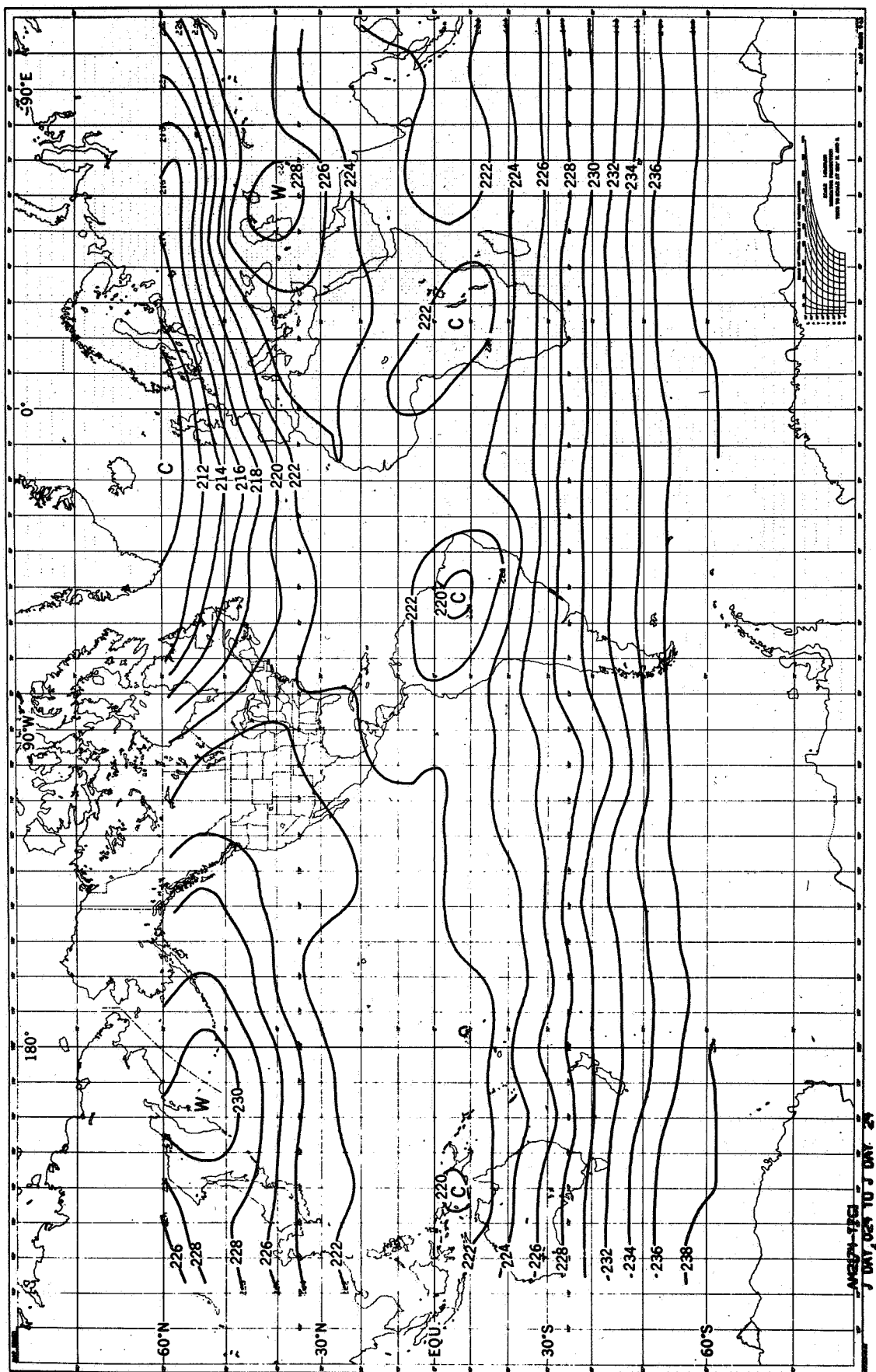
Figure 10—Isotherms for average equivalent blackbody temperatures derived from TIROS VII 15 micron CO_2 band radiation observations during the period 20 Jan. – 29 Jan. 1964. Numbers along the isotherms refer to degrees Kelvin. Radiation observations were restricted to nadir angles 0–40°.
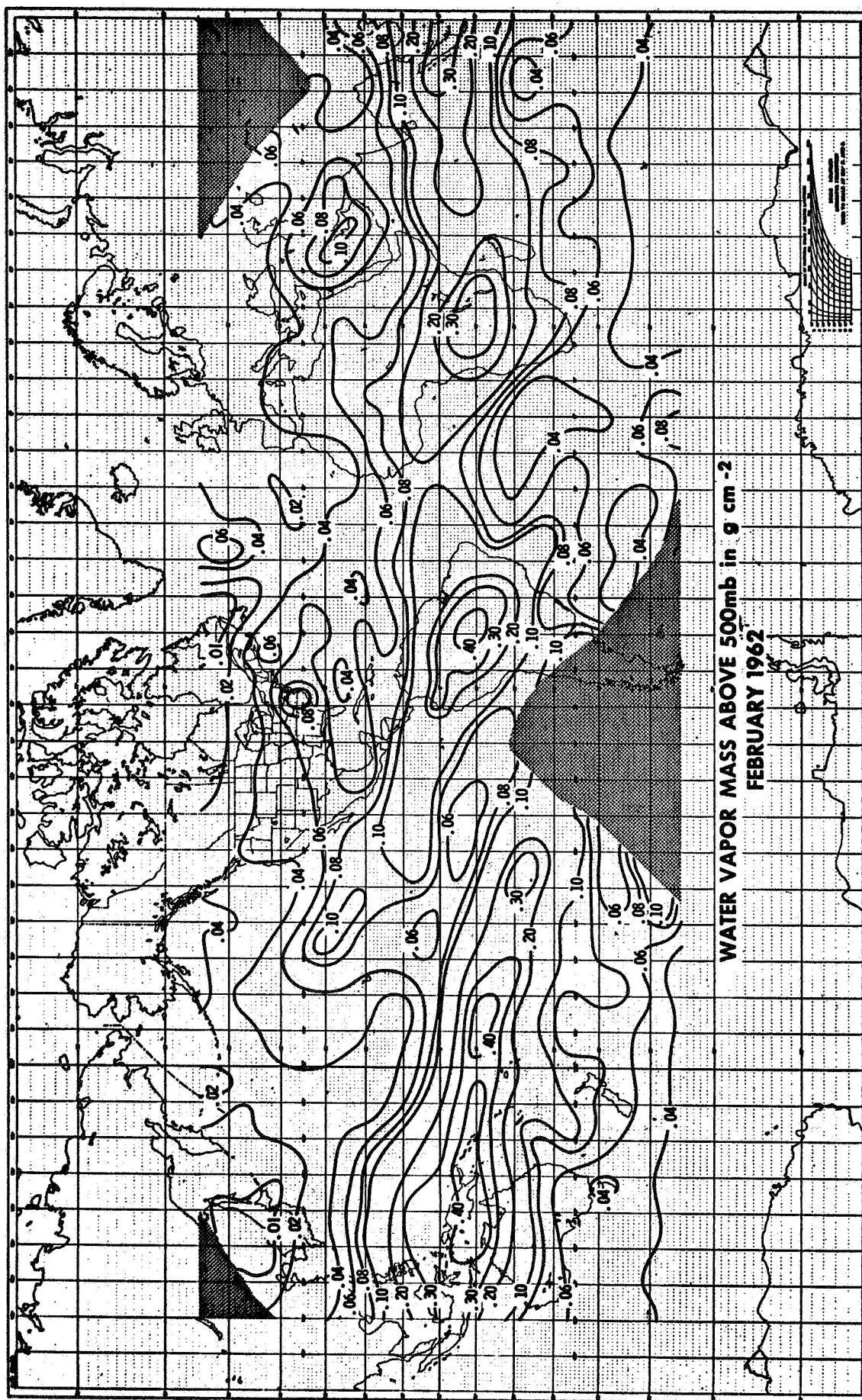
Figure 11—Average water vapor mass above 500 mb in g/cm² for February 1962 derived from measurements in the 6.3 micron water vapor band and in the 11 micron window from TIROS IV.